Anisotropy and Magnetostriction of Iridium-Substituted Yttrium Iron Garnet

P. Hansen, J. Schuldt, and W. Tolksdorf
Philips Forschungslaboratorium Hamburg GmbH, 2 Hamburg 54, Germany
(Received 16 April 1973)

The anisotropy, magnetostriction, and linewidth of iridium-substituted yttrium iron garnet single crystals of the composition $Y_{3-x}A_xFe_{5-y-z}Ir_yB_zO_{12-\delta}F_\delta$ ($A = Ca^{+2}$, Pb^{2+} and $B = Fe^{2+}$, Si^{4+}, Zn^{2+}) have been investigated by means of ferromagnetic resonance. Chemical-analysis data of Ir, Zn, Ca and of the impurities Pb, Si, and F are given for all crystals. The anisotropy and magnetostriction measurements were carried out at 9.15 GHz in the temperature range 4.2–500 K. The anisotropy contributions ΔK_1 and ΔK_2 caused by the low-spin $5d^5$ Ir^{4+} ions are positive with $\Delta K_2 \gg \Delta K_1$ and the magnetostriction contributions $\Delta\lambda_{100}$ and $\Delta\lambda_{111}$ are negative with $|\Delta\lambda_{100}| \gg \Delta\lambda_{111}$. The temperature dependence of both the anisotropy and magnetostriction is compared with calculations performed in the framework of the single-ion theory. The resonance linewidth showing a maximum at $T = 370$ K could be qualitatively interpreted by the longitudinal relaxation model assigning a relaxation time of 10^{-11} sec to the Ir^{4+} ions.

I. INTRODUCTION

Transition-metal ions with a strong spin-orbit coupling substituted in ferrites and garnets are well known to give rise to large changes in the magnetic properties. In particular, the metal ions of the second and third transition series, where the spin-orbit coupling constant ranges between 500 and 2500 cm^{-1}, are expected to contribute significantly to the anisotropy energy

$$F_K(\vec{\alpha}) = K_0 + K_1(\alpha_1^2\alpha_2^2 + \alpha_2^2\alpha_3^2 + \alpha_1^2\alpha_3^2) + K_2\alpha_1^2\alpha_2^2\alpha_3^2 + \cdots \quad (1)$$

and the magnetoelastic energy

$$F_{me}(\vec{\alpha}, \vec{\epsilon}) = b_0(\epsilon_{11}+\epsilon_{22}+\epsilon_{33}) + b_1(\alpha_1^2\epsilon_{11} + \alpha_2^2\epsilon_{22} + \alpha_3^2\epsilon_{33}) + 2b_2(\alpha_1\alpha_2\epsilon_{12} + \alpha_2\alpha_3\epsilon_{23} + \alpha_1\alpha_2\epsilon_{13}) + \cdots, \quad (2)$$

where the α_p are the direction cosines of the magnetization with respect to the cubic axis and ϵ_{pq} are the components of the strain tensor.

Generally for such magnetically strong anisotropic ions the cubic ground state is an orbitally threefold-degenerate T state. The influence of these ions on the anisotropy constants K_1 and K_2 and on the magnetoelastic constants b_1 and b_2 depends on the particular crystallographic sites occupied. Thus octahedral ions lead to a positive and tetrahedral ions to a negative contribution to K_1. The sign of K_2 and of the magnetoelastic constants depend, in addition, on the sign of the local crystalline fields. This is well known for the $3d$ elements Fe^{2+}, Co^{2+} [1–11] and the $4d$ element Ru^{3+} [12–20] and the observed effects are in accordance with theoretical calculations in the framework of the single-ion theory. The only $5d$ ion which has been garnet (YIG). Some anisotropy and ferromagnetic-resonance-linewidth measurements have been reported. [13] The purpose of this paper is an extension of these measurements to higher temperatures and the study of the magnetostrictive effects.

The iridium ions are expected to occupy octahedral sites, owing to their preferred coordination and the ionic radius (0.63 Å [21] for Ir^{4+}). Both Ir^{3+} and Ir^{4+} are in the low-spin state, owing to the large cubic crystalline field. [22] Ir^{3+} with a $5d^6$ configuration has a completely filled t_{2g} shell and therefore is nonmagnetic and should not contribute to the magnetic properties. This behavior could be verified measuring the spin-wave linewidth of iridium-doped polycrystalline garnets. [23] Thus the problem of separating the contribution from ions of different valencies which arises for most of the anisotropic ions will not occur in this case, provided a pure octahedral occupation is present. However, the determination of the small actual concentrations of the Ir^{4+} ions in the measured crystals is still very complicated or impossible. This difficulty is enlarged by the presence of impurities as Ca^{2+}, Pb^{2+}, Fe^{2+}, Si^{4+}, and F^- whose content is of the same order of magnitude.

In Sec. II the contribution of low-spin d^5 ions to the anisotropy and magnetostriction has been calculated within the scope of the single-ion model. In Sec. III these results will be compared with experimental data from chemical analysis, optical-absorption measurements, spin-wave-linewidth data and temperature dependence of the ferromagnetic-resonance linewidth, the resonance field, anisotropy, and magnetostriction constants. The fit of the single-ion theory to the experimental data yields values for the exchange field and the ratio v/ξ, where v is the one-electron trigonal field parameter and ξ is the one-electron spin-orbit coupling parameter.

II. THEORY OF LOW-SPIN d^5 IONS

A. Single-Ion Theory

The contribution from anisotropic ions to the magnetic properties of ferrites and garnets can be well treated in the single-ion theory.[24,25] This requires that these ions will not interact with each other, which will be valid for a sufficient small concentration below 1 at.% of the iron ions on octahedral or tetrahedral sites. However, for practical analysis some further assumptions have to be made.

(i) The same energy conditions should be present for each crystallographic equivalent site. Thus all energies determined by crystalline fields and spin-orbit coupling should be the same for all octahedral or tetrahedral sites. This in particular excludes fluctuations in composition on atomic scale.

(ii) The exchange energy will be treated in terms of the molecular-field approximation. The magnitude of the exchange field should be independent of space and direction and is assumed to be parallel to the direction of magnetization. No anisotropic exchange interaction will be considered and an isotropic g factor is used. In addition we will not account for the strain dependence of the exchange field.

(iii) Mixing of higher cubic energy terms into the ground level will be neglected due to the high-crystalline-field splittings,[30] which is shown in Fig. 1. Further, the overlap of the d electrons of the d^5 ion onto the ligands whose effect is to reduce the orbital angular momentum matrix element[26] will not be taken into account. This effect, which is described by the orbital reduction factor k, does not give rise to significant changes in the anisotropy.[13]

(iv) The influence of the presence of canting of the neighboring iron ions[27,28] will not be introduced in the considerations.

(v) The Coulomb interaction between the Ir^{4+} ions and the charge-compensating ions as Ca^{2+} and Zn^{2+} will be neglected. This effect may be of the order of 100 cm^{-1}.

With these assumptions the single-ion Hamiltonian acting on the wave functions of the cubic ground state can be written in the form

$$\mathcal{H} = V_t(\vec{r}) - \xi \vec{L}\cdot\vec{S} + g\mu_B \vec{H}_e \cdot \vec{S} + \delta V(\vec{r}, \overleftrightarrow{\epsilon}). \tag{3}$$

$V_t(\vec{r})$ is the local crystalline-field energy. The second term represents the spin-orbit coupling where $\vec{L}$ and $\vec{S}$ are the orbital and spin momentum of the d^5 ion. Since the low-spin d^5 configuration t_{2g}^5 corresponds to a hole in the t_{2g} shell, the spin-orbit coupling constant λ has been replaced by the one-electron spin-orbit coupling parameter ξ, where $\lambda = -\xi$. The third term describes the exchange interaction in the molecular-field approximation where g and μ_B are the g factor and the Bohr magneton, respectively. Finally, $\delta V(\vec{r}, \overleftrightarrow{\epsilon})$ is the increment of crystalline-field energy depending on the strain tensor $\overleftrightarrow{\epsilon}$. This term is responsible for the magnetostrictive effects.

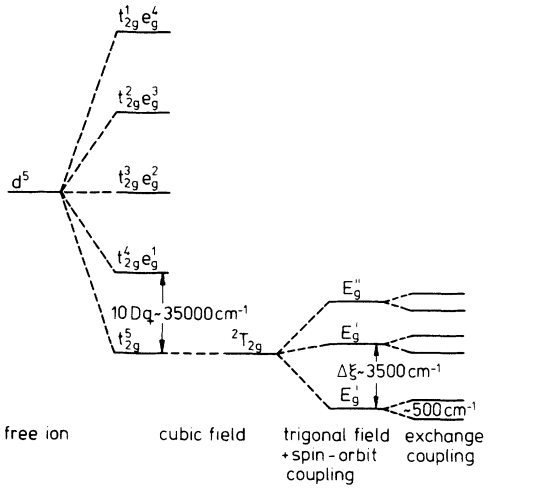

FIG. 1. Energy levels of Ir^{4+} in YIG with a low-spin $5d^5$ configuration. The primed representations are of the double trigonal group. The energy differences are not to scale.

The relative magnitude of the energy terms and their influence on the level splitting is shown schematically in Fig. 1.

B. Anisotropy

Assuming the d^5 ions to be statistically distributed over the magnetically inequivalent sites, the free energy per unit volume can be expressed by

$$\Delta F(\vec{\alpha}) = -\frac{kTN}{r}\sum_{n=1}^{r} \ln Z_n,$$
$$Z_n = \sum_m e^{-E_{nm}(\vec{\alpha})/kT}, \tag{4}$$

where k, T, and N are the Boltzmann constant, the temperature and the total number of d^5 ions per cm^3, respectively. r denotes the number of inequivalent sites, where $r = 4$ for octahedral sites and $r = 3$ for tetrahedral sites. Z_n is the partition function and the sum carries over all energy levels $E_{nm}(\vec{\alpha})$ of the ion on site n, depending on the direction of magnetization $\vec{\alpha}$. An expansion of $\Delta F(\vec{\alpha})$ in powers of α_i according to Eq. (1) is only possible in the limiting cases[16] $T = 0$ K and $kT \gg E_{nm+1}(\vec{\alpha}) - E_{nm}(\vec{\alpha})$ for small m.[14] The complete temperature dependence of the anisotropy contributions ΔK_1 and ΔK_2 therefore is deduced from the free energy of Eq. (4) in the principal directions. From Eq. (1) the relations

$$\Delta K_1 = 4(\Delta F[110] - \Delta F[001]),$$
$$\Delta K_2 = 9(3\Delta F[111] + \Delta F[001] - 4\Delta F[110]) \tag{5}$$

can be easily verified if higher-order anisotropy terms are neglected.

The dependence of the energy levels E_{nm} on the direction of magnetization will be obtained applying the single-ion Hamiltonian of Eq. (3) on a suitable set of wave functions of the sixfold-degenerate $^2T_{2g}$ cubic ground state. The quantization axis on octahedral sites is chosen along the trigonal axis being one of the [111] directions and on tetrahedral sites along one of the [100] directions. For the case that the spin-orbit coupling is large as compared with the exchange energy, an assumption which is valid for the present case, the Hamiltonian (3) becomes diagonal within the following set of wave functions:

$$\begin{aligned}
\Phi_1^{\pm} &= a_{\pm}(\pm c_{\pm} t_3^{+} + c_{\mp} t_1^{-})\, e^{-i\delta_n/2} \\
&\quad - b_{\pm}(\mp c_{\pm} t_3^{-} + c_{\mp} t_2^{+})\, e^{i\delta_n/2}, \\
\Phi_2^{\pm} &= b_{\pm}(\pm c_{\pm} t_3^{+} + c_{\mp} t_1^{-})\, e^{-i\delta_n/2} \\
&\quad + a_{\pm}(\pm c_{\pm} t_3^{-} + c_{\mp} t_2^{+})\, e^{i\delta_n/2}, \\
\Phi_{1/2}^{0} &= t_{1/2}^{\pm}\,.
\end{aligned} \tag{6}$$

The $t_k^{\pm}$ are linear combinations of the d functions which are quantized along the trigonal or tetragonal axis.[14,29] The coefficients are defined by

$$a_{\pm}^2 = \frac{1}{2}\left(1 \mp \frac{(1-2c_{+}^2)\cos\gamma_n}{[(1-2c_{+}^2)^2\cos^2\gamma_n + c_{\pm}^4\sin^2\gamma_n]^{1/2}}\right),$$

$$a_{\pm}^2 + b_{\pm}^2 = 1, \quad c_{+}^2 = \frac{1}{2}\left(1 - \frac{\frac{1}{2} - v/\xi}{[2 + (\frac{1}{2} - v/\xi)^2]^{1/2}}\right),$$

$$c_{+}^2 + c_{-}^2 = 1. \tag{7}$$

v is the single-ion trigonal field parameter.[16] γ_n and δ_n are the angles between the direction of magnetization and the nth quantization axis. The corresponding energies are of the form

$$\begin{aligned}
E_{1/2}^{+} &= E_{+} \pm \tfrac{1}{2} g\mu_B H_e \\
&\quad \times \{c_{+}^4 + [(1-2c_{+}^2)^2 - c_{+}^4]\cos^2\gamma_n\}^{1/2}, \\
E_{1/2}^{-} &= E_{-} \pm \tfrac{1}{2} g\mu_B H_e \\
&\quad \times \{c_{-}^4 + [(1-2c_{+}^2)^2 - c_{-}^4]\cos^2\gamma_n\}, \\
E_{1/2}^{0} &= E_0 \pm \tfrac{1}{2} g\mu_B H_e \cos\gamma_n\,,
\end{aligned} \tag{8}$$

where the terms E_0 and $E_{\pm}$ depend only on v and ξ[13,26] and thus do not contribute to the anisotropy. Further, the strain-dependent part of the crystalline field is neglected. $E_{1/2}^{+}$ represents the lowest magnetic doublet irrespective of magnitude and sign of v/ξ, while $E_{1/2}^{-} > E_{1/2}^{0}$ for $v/\xi < 0$ and $E_{1/2}^{-} < E_{1/2}^{0}$ for $v/\xi > 0$. In the limit $H_e \to 0$ and $v/\xi = 0$ the four energy levels $E_{1/2}^{0}$ and $E_{1/2}^{-}$ are degenerate, since then $E_{-} = E_0$. Therefore the level splitting of these four energies become quite complicated in the range $v/\xi \approx 0$ and then the wave functions $\Phi_{1/2}^{-}$ and $\Phi_{1/2}^{0}$ are not accurate. However, this is not very important concerning the anisotropy contribution which is governed by $\Phi_{1/2}^{+}$ and approximately not affected by these higher levels.

Combining Eqs. (4), (5), and (8), ΔK_1 and ΔK_2 can be written[10]

$$\Delta K_1 = 2kTN\left\{\ln\left[\cosh^2\left(\frac{E_e}{kT}\right) \Big/ \cosh\left(\frac{E_e(1+\epsilon)^{1/2}}{kT}\right)\cosh\left(\frac{E_e(1-\epsilon)^{1/2}}{kT}\right)\right] + \eta_1(T)\right\},$$

$$\begin{aligned}
\Delta K_2 = \frac{9kTN}{4}\Bigg\{&\ln\Bigg[\cosh^8\left(\frac{E_e(1+\epsilon)^{1/2}}{kT}\right)\cosh^8\left(\frac{E_e(1-\epsilon)^{1/2}}{kT}\right) \Big/ \cosh^4\left(\frac{E_e}{kT}\right)\cosh^3\left(\frac{E_e(1-2\epsilon)^{1/2}}{kT}\right) \\
&\times \cosh^9\left(\frac{E_e(1+\tfrac{2}{3}\epsilon)^{1/2}}{kT}\right)\Bigg] + \eta_2(T)\Bigg\},
\end{aligned} \tag{9}$$

where

$$E_e = \frac{g\mu_B H_e[2c_{+}^2 + (1-2c_{+}^2)^2]^{1/2}}{2\sqrt{3}}\,,$$

$$\epsilon = \frac{c_{+}^4 - (1-2c_{+}^2)^2}{2c_{+}^2 + (1-2c_{+}^2)^2}\,. \tag{10}$$

The terms $\eta_1(T)$ and $\eta_2(T)$ are due to the effect of the higher levels. They will be proportional to $\exp(-|E_{-} - E_{+}|/kT)$ or $\exp(-|E_0 - E_{+}|/kT)$.[16] For Ru^{3+} in YIG and GdIG this term contributes about 5% and the same holds for Ir^{4+} in YIG. The ratio $\Delta K_2/\Delta K_1$ is independent of concentration. In addition, for $T = 0$ K it becomes independent on the exchange field and then is only governed by v/ξ. A plot $\Delta K_2/\Delta K_1$ vs v/ξ is given in Fig. 2. Experimental values representing average values from various compositions of $Ru^{3+}(4d^5)$ in YIG[17] and in GdIG[16] and $Ir^{4+}(5d^5)$ in YIG[30] indicate the possibility of estimating v/ξ. For comparison, $\Delta K_2/\Delta K_1$ for a low-spin d^5 ion on tetradhedral sites[17] is shown. v then represents the tetragonal field splitting.

Generally at very low temperatures the influence of higher-order anisotropy constants becomes quite important and then the relations (9) are not accurate. This suggests consideration of the field for ferromagnetic resonance

$$H_r = -\tfrac{1}{2}(H_K^x + H_K^y) + [\tfrac{1}{4}(H_K^x - H_K^y)^2 + (\omega/\gamma)^2]^{1/2}, \tag{11}$$

since it can be deduced from the free energy without neglecting higher-order anisotropy terms. H_K^x and H_K^y refer to a coordinate system in which the applied magnetic field is parallel to the z axis. The anisotropy field $\vec{H}_K$ consists of the part $\vec{H}_K^0$ of the undoped material that can be derived from Eq. (1) and the contribution $\delta\vec{H}_K$ of the low-spin d^5 ion which can be calculated from Eqs. (4). ω and γ are the measuring frequency and the gyromagnetic ratio, respectively. $\delta\vec{H}_K$ can be written for the principal directions of magnetization for octhaderal sites as follows[10,16]:

$$\delta H_K^x[001] = \delta H_K^y[001] = \frac{NE_e\epsilon^2}{M_s}\left[\tanh\left(\frac{E_e}{kT}\right) - \frac{E_e}{kT\omega_{[001]}\cosh^2(E_e/kT)}\right],$$

$$\delta H_K^x[111] = \delta H_K^y[111] = \frac{3}{4}\frac{NE_e\epsilon}{M_s}\left[-\tanh\frac{E_e(1-2\epsilon)^{1/2}}{(1-2\epsilon)^{1/2}} + \frac{1+\frac{10}{9}\epsilon}{(1+\frac{2}{3}\epsilon)^{3/2}}\tanh\left(\frac{E_e(1+\frac{2}{3}\epsilon)^{1/2}}{kT}\right) - \frac{4}{9}\frac{E_e\epsilon}{kT\omega_{[111]}\cosh^2[E_e(1+\frac{2}{3}\epsilon)^{1/2}/kT]}\right], \tag{12}$$

$$\delta H_K^x[110] = \frac{1}{2}\frac{NE_e\epsilon}{M_s}\left(\frac{\tanh[E_e(1+\epsilon)^{1/2}/kT]}{(1+\epsilon)^{1/2}} - \frac{1-3\epsilon}{(1-\epsilon)^{3/2}}\tanh[E_e(1-\epsilon)^{1/2}/kT] - \frac{2E_e\epsilon}{kT\omega_{[110]}\cosh^2[E_e(1-\epsilon)^{1/2}/kT]}\right),$$

$$\delta H_K^y[110] = \frac{NE_e\epsilon}{M_s}\left(\frac{\tanh[E_e(1+\epsilon)^{1/2}/kT]}{(1+\epsilon)^{1/2}} - \frac{\tanh[E_e(1-\epsilon)^{1/2}/kT]}{(1-\epsilon)^{1/2}}\right),$$

where

$$\omega_{[hkl]} = 1 + (\omega\tau_{[hkl]})^2.$$

$\tau_{[hkl]}$ is the thermal relaxation time between the two lowest levels of the d^5 ion. Similar relations can be deduced for the tetrahedral case. At low temperatures any ratio of the resonance fields becomes independent of concentration and exchange field and is therefore a suitable measure for v/ξ.

C. Magnetostriction

The magnetoelastic energy $F_{me}(\vec{\alpha}, \vec{\epsilon})$ depends on the direction of magnetization and the strain tensor and can be described in many cases by two phenomenological constants b_1 and b_2 according to Eq. (2). These are related to the magnetostriction constants λ_{100} and λ_{111} by

$$\lambda_{100} = -\frac{2}{3}\frac{b_1}{C_{11}-C_{12}}, \qquad \lambda_{111} = -\frac{1}{3}\frac{b_2}{C_{44}}, \tag{13}$$

where C_{11}, C_{12}, and C_{44} are the elastic constants. Introducing the functions

$$f_{pq}(\vec{\alpha}) = \frac{\partial\Delta F}{\partial\epsilon_{pq}}, \tag{14}$$

the contributions $\Delta\lambda_{100}$ and $\Delta\lambda_{111}$ to the magnetostriction constants are related to these functions $f_{pq}(\vec{\alpha})$ evaluated in certain crystallographic directions of the magnetization

$$\Delta\lambda_{100} = \frac{2(f_{33}[010] - f_{33}[001])}{3(C_{11}-C_{12})},$$

$$\Delta\lambda_{111} = -\frac{1}{3}\frac{f_{12}[110]}{C_{44}}. \tag{15}$$

$p, q = 1, 2, 3$ refer to the cubic axes x, y, z, respectively. Similar to the case of the anisotropy, these relations are only valid if the two-constant theory of Eq. (2) without further magnetoelastic constants can be applied.

The influence of low-spin d^5 ions originates from the last term of the Hamiltonian of Eq. (3). To calculate this strain dependence on the free energy ΔF we expand the partition function Z_n[31]:

$$Z_n = Z_{n0} + \sum_{l=1}^{\infty} Z_{nl},$$

where Z_{n0} is given by the second relation of Eqs. (4). Z_{nl} depend on the matrix elements of crystal-field operator $\delta V(\vec{r}, \vec{\epsilon})$,[7,31] with wave functions given in Eqs. (6).[20] In the case $(\xi/g\mu_B H_e)^2 \gg 1$, $\Delta\lambda_{100}$, and $\Delta\lambda_{111}$ can be expressed by

$$\lambda_{100} = \frac{4}{3}\frac{NW_{33}G^0}{C_{11}-C_{12}} \times \left\{\left[c_+^2 + E_e\left(\frac{G^0}{\Delta_\xi^0} + \frac{G_1^-}{\Delta_\xi^-}\right)\right]\tanh\left(\frac{E_e}{kT}\right) + E_e\left(\frac{1}{\Delta_\xi^0} + \frac{G_2^-}{\Delta_\xi^-}\right)\right\},$$

$$\lambda_{111} = \frac{1}{6}\frac{NW_{12}E_e(G^0)^2}{C_{44}\,\Delta_\xi^0} \times \left(\frac{3\tanh[E_e(1+\epsilon)^{1/2}/kT]}{(1+\epsilon)^{1/2}} + \frac{\tanh[E_e(1-\epsilon)^{1/2}/kT]}{(1-\epsilon)^{1/2}}\right), \tag{16}$$

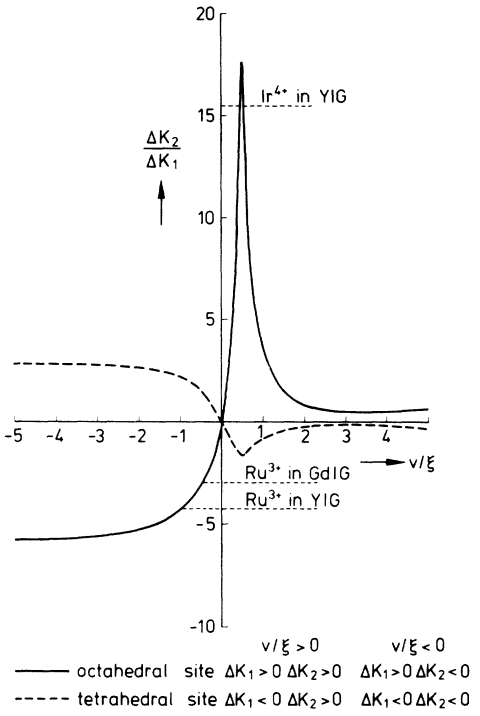

FIG. 2. The ratio $\Delta K_2/\Delta K_1$ of the anisotropy contributions of a low-spin d^5 ion on tetrahedral and octahedral sites at $T=0$ K. Average experimental values for Ru^{3+} in YIG (Ref. 14) and GdIG (Ref. 16) and Ir^{4+} in YIG (Ref. 30) are indicated.

where $\Delta_\xi^0 = E_0 - E_+$ and $\Delta_\xi^- = E_- - E_+$. G^0, G_1^-, and G_2^- are functions of v/ξ. ϵ and E_e are given in Eqs. (10). W_{12} and W_{33} are matrix elements defined as

$$W_{12} = \frac{\partial}{\partial \epsilon_{12}} \langle t_1 | \delta V_1(\vec{r}, \overleftrightarrow{\epsilon}) | t_3 \rangle ,$$
$$W_{33} = \frac{\partial}{\partial \epsilon_{33}} \langle t_1 | \delta V_n(\vec{r}, \overleftrightarrow{\epsilon}) | t_2 \rangle . \tag{17}$$

$\delta V_n(\vec{r}, \overleftrightarrow{\epsilon})$ represents the crystal-field operator in the $x_n y_n z_n$ system, where $\vec{z}_1 \| [111]$, $\vec{z}_2 \| [\bar{1}\bar{1}1]$, $\vec{z}_3 \| [\bar{1}11]$, $\vec{z}_4 \| [1\bar{1}\bar{1}]$, and $\vec{z}_n$ is the unit vector along the z_n axis.

If the condition $(\xi/g\mu_B H_e)^2 \gg 1$ is not fulfilled, the expressions for $\Delta\lambda_{100}$ and $\Delta\lambda_{111}$ become very lengthy[20] and will not be given here. They are plotted in Figs. 3(a) and 3(b) versus v/ξ at $T=0$ K. Thus very strong effects are predicted in the range of expected v/ξ values for low-spin d^5 ions. It should be pointed out that the normalizing factors $n_{100} = NW_{33}/(C_{11} - C_{12})$ and $n_{111} = NW_{12}/C_{44}$ change sign if the trigonal field energy

$$V(\vec{r}, \overleftrightarrow{\epsilon}) \cong V(\vec{r}) + \sum_{p \le q} V_{pq}(\vec{r}) \epsilon_{pq}$$

changes the sign.

The values at $v/\xi \approx 0$ give only an estimate of $\Delta\lambda_{100}$ and $\Delta\lambda_{111}$, since the wave functions (6) are not accurate in this limit. The same holds for $g\mu_B H_e/\xi \gtrsim 0.5$ because for $g\mu_B H_e \approx \xi$ the complete six-dimensional problem has to be solved.

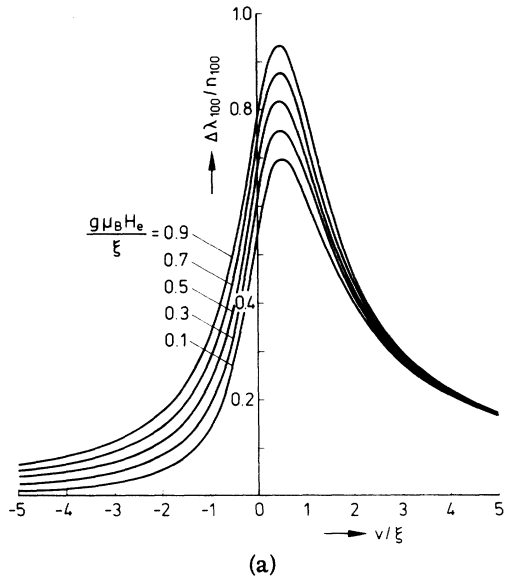

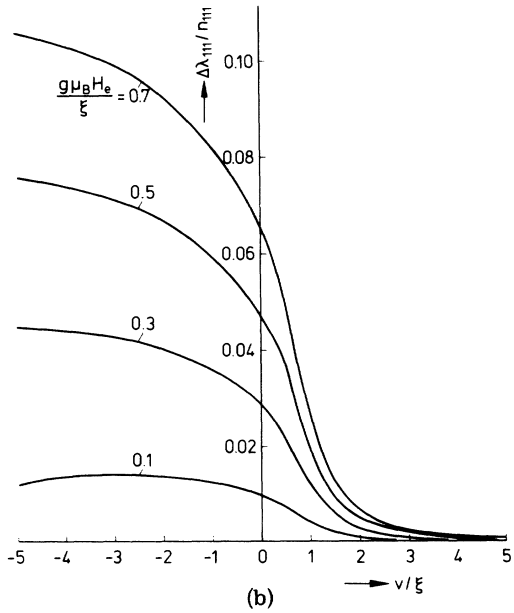

FIG. 3. The normalized magnetostriction contributions (a) $\Delta\lambda_{100}/n_{100}$ and (b) $\Delta\lambda_{111}/n_{111}$ for a low-spin d^5 ion on an octahedral site at $T=0$ K. n_{100} and n_{111} denote $NW_{33}/(C_{11} - C_{12})$ and NW_{12}/C_{44}, respectively.

III. EXPERIMENTS AND DISCUSSION

A. Growth of Single Crystals and Optical Absorption

Single crystals were grown with a cooling rate of 0.5 °C/h in a flux in the temperature range 1120–1000 °C, where they were separated from the flux by turning the platinum crucible upside down[32,33]; 150-g melt were used with the composition in weight percent: PbO: 36.3; PbF_2: 27.0; B_2O_3: 5.4; Fe_2O_3: 3.5 and 27.8 oxides forming $Y_{3-x}Ca_xFe_{5-y-z}Ir_yZn_zO_{12}$. The values of the starting composition x_0, y_0, and z_0 are given in Table I together with the values actually analyzed in the crystals. Impurities of Ca and Si of the order of 10 ppm by weight were present in the flux materials. Y_2O_3 was of 99.9999% pure with respect to the rare earth. The yield was about 13 g, consisting of several regularly shaped crystals up to 8 mm in size. Inclusion-free samples have been selected for all measurements. Zinc was analyzed by atomic absorption. The analysis of the impurities Pb, Pt, Ca, Si, Fe^{2+} and F has been described previously.[4,33] In Table I the total content of Pb ions was assumed to be divalent. Electron-spin-resonance measurements in diamagnetic garnets, however, indicate that a part of them may be present in the trivalent state.[34] The given errors include the inhomogeneity of the distribution of the ions.

The iridium content was measured directly on polished platelets by x-ray-fluorescence analysis using dense polycrystalline garnet materials for calibration. It should be noted that the iridium substitution was neither reproducible nor very homogeneous, since iridium oxide reacted with the platinum of the crucible. From Table I it becomes apparent that the concentration of iridium ions and the impurities is of the same magnitude. In general, the condition of charge compensation would yield the actual Ir^{4+} content, but in this particular case the accuracy of the values in Table I is not sufficient to make a reliable prediction. The actual Ir^{4+} content in the crystals would be important, since these ions cause the effect on the optical absorption and the magnetic properties.

These polished platelets then were used for the optical measurements and for milling spheres for the magnetic studies. The optical-transmission measurements were carried out with platelets of 1-mm thickness in the wavelength range of 1.1–2.5 μm with a Zeiss PMQII spectrophotometer. In Fig. 4 the absorption coefficients $\alpha' = 0.43\alpha$ is plotted versus wavelength for samples No. 1, 3, and 4. α has been calculated from the transmission measurements according to the relation $I/I_0 = e^{-\alpha D}$ where D is the thickness of the platelet. I/I_0 is the relative intensity of the light corrected with respect to two interface reflections with a reflection coefficient of $R = 0.14$ at 2 μm and a refractive index of $n = 2.188$.[35] The main absorption peak appears at 2.07 μm, which corresponds to 4600 cm^{-1}. The magnitude of the peak increases with the Ir^{4+} concentration and can be used as a relative measure. For single crystals of composition $Y_3Ga_{5-y-z}Ir_yZn_zO_{12}$ this peak is shifted to 1.97 μm. The peak indicates transitions within the manifold of the $^2T_{2g}$ cubic ground state. From the ratio of the energy differences $\Delta_\xi^0/\Delta_\xi^-$, which depends on v/ξ, the second level should occur about 3500 cm^{-1} above the ground level (see Fig. 1), since $|v/\xi|$ is expected to range around 0.5.

Absorption measurements with samples of about 100-μm thickness showed in addition an increase of α with respect to the Ir^{4+} concentration in the range 0.7–1 μm.

B. Resonance Measurements

The anisotropy, linewidth, and magnetostriction measurements of the single crystals have been carried out by means of the ferromagnetic-resonance method at about 9.15 GHz and in the temperature range 4.2–500 K. Spheres of 0.7-mm diameter were used and oriented in a $(\bar{1}10)$ plane with an accuracy of 0.5°. The resonance apparatus has been supplied with an automatic recording of the field for resonance.[36] A block diagram of the equipment is shown in Fig. 5. The resonance field can be plotted automatically with different velocities as a function of orientation without or with a compressional stress on the sphere or as a

TABLE I. Analysis of single crystals of composition $Y_{3-x}A_xFe_{5-y-z}Ir_yB_zO_{12-\delta}F_\delta$. $A = Ca^{2+}$, Pb^{2+} and $B = Zn^{2+}$, Fe^{2+}, Si^{4+}. x_0, y_0, and z_0 refer to the starting composition.

	x		y	z			δ	x_0	y_0	z_0
Sample	Ca^{2+}	Pb^{2+}	$Ir^{3+}+Ir^{4+}$	Si^{4+}	Zn^{2+}	Fe^{2+}	F^-	Ca^2	Ir^{4+}	Zn^{2+}
No. 1	0.0010	0.015	0	0.002	0	0.006		0	0	0
No. 2	0.0014	0.013	0.0026	0.006	0	0.005		0	0.02	0
No. 3	0.0012	0.013	0.004	0.001	0.003	0.004	0.01	0	0.02	0.06
No. 4	0.0012	0.015	0.0078	0.002	0.001	0.007		0	0.02	0.02
No. 5	0.0067	•••	0.038	•••	0	•••		0.05	0.05	0
error	±0.0005	±0.002	±0.0015	±0.001	±0.0005	±0.004	±0.003	•••	•••	•••

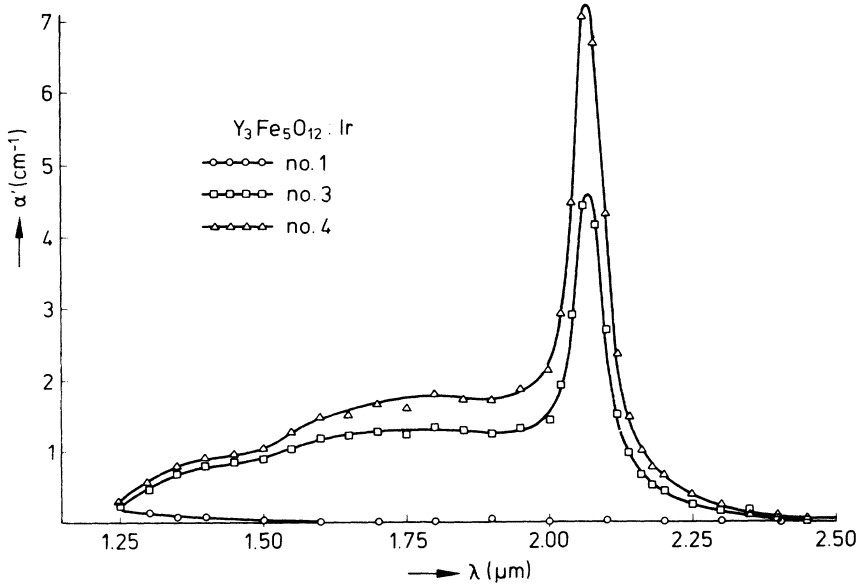

FIG. 4. Optical absorption of iridium-substituted YIG single crystals. α' is defined by $\alpha' = 0.43\alpha = (0.43/D)\ln(I_0/I)$. The strong peak at $\lambda = 2.07$ μm is caused by the presence of Ir^{4+} ions arising from transitions within the $^2T_{2g}$ manifold.

function of temperature. For linewidth measurements the transmitted power is written versus field. The resolution in field is 0.25 Oe, determining the accuracy and limit of the linewidth and magnetostriction measurements.

This method improves the accuracy of the resonance measurements and allows a much quicker evaluation of the anisotropy data. A resonance curve through 360° can be plotted usually within 1 min. Only in exceptional cases of small linewidth and very large anisotropies, longer times are required.

In Fig. 6 the continuously plotted resonance field is shown for sample No. 3 at different temperatures. The drastic change of the curvature becomes apparent and is caused by the presence of a large positive K_2 shifting the easy direction of magnetization from [111] to [110] direction for $K_2 > -\frac{4}{9} K_1$. For sample No. 3 this condition is fulfilled for temperatures below 120 K.

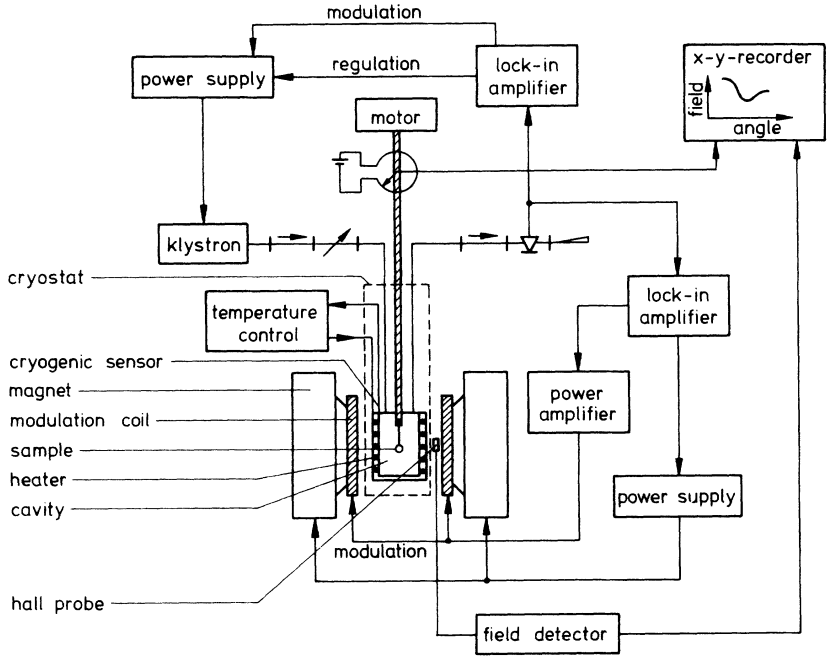

FIG. 5. Block diagram of the electronic equipment for the resonance measurements.

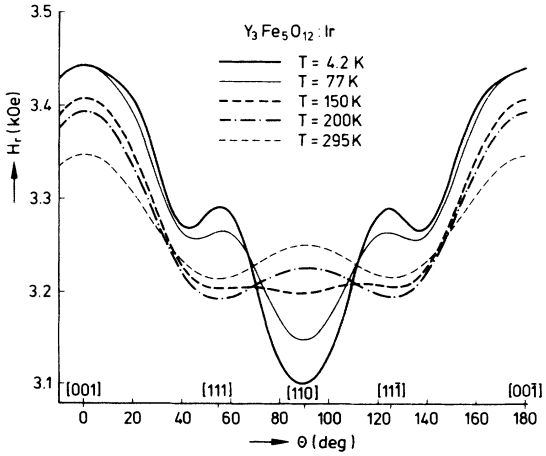

FIG. 6. The orientation dependence of the field for ferromagnetic resonance in a ($\bar{1}$10) plane for different temperatures for sample No. 3. The strong influence of the Ir^{4+} ions at low temperatures become obvious, resulting in an easy direction of magnetization along [110].

Neglecting higher-order terms in Eq. (1), K_1/M_s and K_2/M_s were obtained from the field for resonance in the three principal directions using the relations

$$\begin{aligned}
&\omega/\gamma = H_r[001] + 2K_1/M_s,\\
&\omega/\gamma = H_r[111] - \tfrac{4}{3}K_1/M_s - \tfrac{4}{9}K_2/M_s,\\
&\omega/\gamma = (H_r[110] - 2K_1/M_s)^{1/2}\\
&\qquad \times (H_r[110] + K_1/M_s + \tfrac{1}{2}K_2/M_s)^{1/2},
\end{aligned} \tag{18}$$

where $H_r[hkl]$ is the field for resonance in the $[hkl]$ direction in a ($\bar{1}$10) plane. The values obtained for sample nos. 1–5 are given in Fig. 7. The change in K_1/M_s is very small and therefore the values for sample nos. 4 and 5 have been omitted. The contributions $\Delta(K_1/M_s)$ and $\Delta(K_2/M_s)$ of the Ir^{4+} ions appear to be positive, indicating $v/\xi > 0$ [13] in contrast to Ru^{3+} in YIG. The decrease of $\Delta(K_2/M_s)$ with temperature is very strong and the anisotropy effect becomes small above room temperature for our small substitutions.

Measurements of the saturation magnetization have been made with a vibrating sample magnetometer, showing for small samples the values of pure YIG which were expected for these small substitutions. Thus ΔK_1 and ΔK_2 can be calculated and the result is displayed in Fig. 8 for sample No. 3. Using the formulas (9) with $\eta_1(T) = \eta_2(T) = 0$, a good fit of the experimental data could be achieved yielding the values $v/\xi = 0.49$, $gH_e = 2.2\times10^7$ Oe, and $y_{Ir^{+4}} = 0.0002$. The temperature dependence of the exchange field according to the molecular-field theory[37,38] has been taken into account, since it becomes very important above room temperature. The values of the atomic parameters only can be

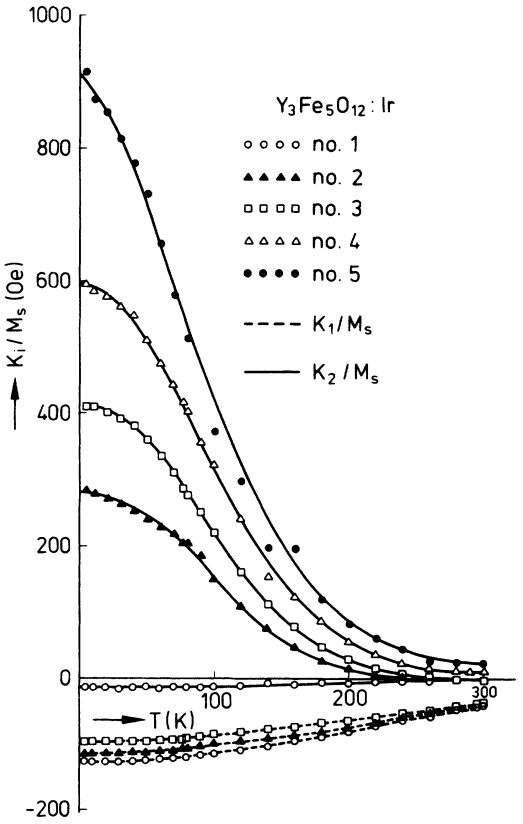

FIG. 7. Temperature dependence of K_1/M_s and K_2/M_s.

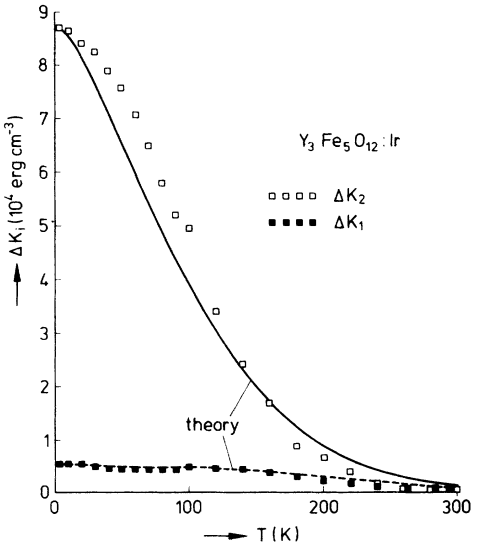

FIG. 8. Temperature dependence of ΔK_1 and ΔK_2, owing to the presence of Ir^{4+} ions for sample No. 3. The theoretical curves are based on the values $v/\xi = 0.494$ and $gH_e = 2.2\times10^7$ Oe.

regarded as a rough estimate because the higher-order anisotropy terms which we have neglected are quite important at low temperatures. In this particular case this is true except for v/ξ , since a change of $\Delta K_2/\Delta K_1$ by a factor of 2 will not give rise for an essential variation of v/ξ as can be seen from Fig. 2.

More reliable values for the atomic parameters will, in general, be expected from the fit of the temperature dependence of the resonance field. For sample No. 3 the resonance fields in the three principal directions are shown in Fig. 9. To adjust the theoretical Eqs. (11) and (12) it is suitable to consider the quantities $\delta H_r[001]/\delta H_r[111]$ or $\delta H_r[001]/(\delta H_r^x[110]+\delta H_r^y[110])$, since they only depend on v/ξ. The best fit for the latter yields $v/\xi = 0.5$. Then, adjusting the resonance field in [001] direction, a concentration $N = 1.7\times10^{18}$ cm^{-3} was obtained. The complete temperature dependence of the theoretical curves of $H_r[011]$ and $H_r[110]$ displayed in Fig. 9 was calculated using the parameters $gH_e = 1.8\times10^7$ Oe and $\tau^0_{[110]} \cong 0.3\tau^0_{[001]} = 0.9\times10^{-11}$ sec. The relaxation times could be deduced fitting both the resonance field and the linewidth simultaneously.

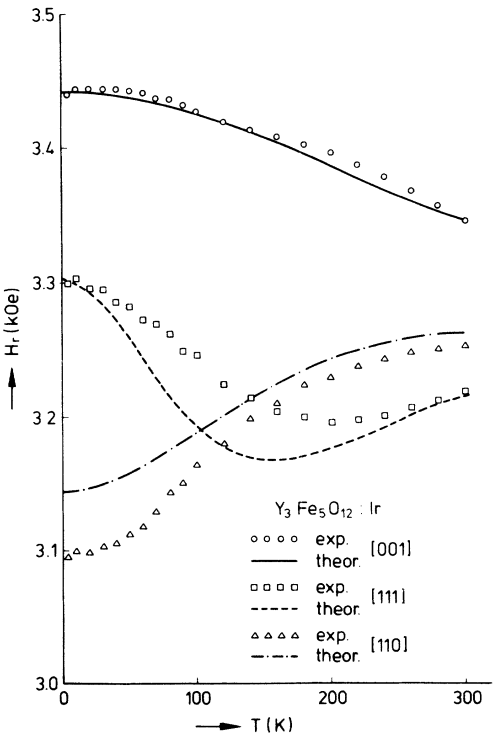

FIG. 9. Temperature dependence of the field for resonance in the principal directions. The theoretical curves have been calculated using the values $v/\xi = 0.5$, $gH_e = 1.8\times10^7$ Oe, and $\tau^0_{[110]} \cong 0.3\tau^0_{[001]} = 0.9\times10^{-11}$ sec.

TABLE II. Linewidth and spin-wave linewidth in [001] direction at 9.15 GHz and $T = 295$ K. The concentration of Ir^{4+} ions has been estimated from the fit of the field for resonance.

Sample	$y_{Ir^{4+}}$	ΔH_k (Oe)	ΔH (Oe)
No. 1	0	0.16	0.9
No. 2	0.0003	4.1	6.5
No. 3	0.0004	5.8	9.5
No. 4	0.0007	8.7	12.0
No. 5	0.0013	16.0	27.0

At $v/\xi = \frac{1}{2}$ ($\epsilon = \frac{1}{2}$) the exchange splitting for $\vec{M}\parallel[111]$ accidently vanishes within the framework of the first-order theory, which leads to very high values in the first term of $\delta H_r[111]$ at low temperatures. Actually, second-order effects or any other interaction, as for instance the Coulomb attraction between Ir^{4+} and a divalent ion, will tend to remove this degeneracy resulting in a finite energy splitting. Assuming a splitting of 80 cm^{-1} the theoretical curve of $H_r[111]$ was calculated.

As can be seen from Fig. 9 a complete agreement with the experimental data could not be achieved. However, the main features of the resonance curves can be described by the simple theory. The value of 80 cm^{-1} is expected to give a rough estimate of the magnitude of other effects and interactions acting on the level splitting. This value has to be compared with about 400 cm^{-1} of the exchange splitting and thus turns out to be not negligible. Therefore the remaining discrepancy between theory and experiment may be caused by these effects or a distribution of the Ir^{4+} ions over different sites. However, if they were involved in the theory, further parameters would enter in the final results, which have, in addition, to be fitted, and this procedure would not improve the accuracy of the determination of the atomic parameters discussed before.

The resonance fields of the other samples could be adjusted similarly. In particular, from the fit of $H_r[001]$ the concentration of Ir^{4+} ions could be estimated and are given in Table II. The increase of the relative concentrations agree well with the observed optical absorption and the measured spin-wave-linewidth data,but the absolute values are very small and we therefore obtain very large anisotropy values per ion (values in the brackets of Table III), which are compared with other strong anisotropic ions in Table III.

C. Resonance Linewidth

The ferromagnetic-resonance linewidth ΔH and spin-wave linewidth ΔH_k is expected to be strongly influenced by the Ir^{4+} ions owing to the orientation dependence of the lowest energy levels. The effect should linearly increase with the concentration.

TABLE III. Influence of octahedral transition-metal ions on the anisotropy and magnetostriction constants of yttrium iron garnet. The values in the brackets refer to the concentrations given in Table II.

Ion	Configuration	Ground state	T (K)	Anisotropy $\Delta K_1/N$ (cm^{-1})	Anisotropy $\Delta K_2/N$ (cm^{-1})	Ref.	Magnetostriction $10^4\Delta\lambda_{100/y}$	Magnetostriction $10^4\Delta\lambda_{111/y}$	Ref.
			4.2	4.5	−17		•••	•••	
Fe^{2+}	$3d^6$	$^5T_{2g}$	77	2.3	−4.1	4	2.7	6.3	4
			295	0.1	−0.1		0.5	1.4	
			4.2	29	−100		•••	•••	
Co^{2+}	$3d^7$	$^4T_{1g}$	77	20	−62	9, 11	•••	•••	11
			295	0.4	−0.2		0	0.5	
			4.2	28	−120		2.7	2.9	
Ru^{3+}	$4d^5$	$^2T_{2g}$	77	22	−68	16, 17	2.7	2.6	19, 20
			295	2	−3		2.5	0.8	
			4.2	1.6(16)	26(260)		−5.1(51)	~−0.2(−2)	
Ir^{4+}	$5d^5$	$^2T_{2g}$	77	1.5(15)	18(180)	present	−4.8(−48)	~−0.1(−1)	present
			295	0.2(2)	0.1(1)	work	−1.9(19)	0	work

This is confirmed by the room-temperature values of ΔH_k and ΔH in [001] direction, which are summarized in Table II. The temperature dependence of the total linewidth $\Delta H[hkl] = \Delta H_0[hkl] + \Delta H_{Ir^{4+}}[hkl]$ in [001] and [111] direction is given in Fig. 10 for sample No. 3, where $\Delta H_0[hkl]$ denotes the linewidth of the unsubstituted YIG. A broad maximum appears at about 370 K. The small peak at low temperatures originates from the small Fe^{2+} content which becomes obvious from the temperature dependence of $\Delta H_0[001]$. Since the Fe^{2+} concentration is of the same magnitude for all samples (see Table I), it does not influence the interpretation of the iridium effect. The linewidth in [110] direction was found to be approximately equal to that in [001] direction and has been omitted in Fig. 10. The orientation dependence turns out to be quite small. All spheres show the same behavior except in absolute magnitude.

Two models have been proposed and extensively discussed to explain the ferromagnetic-resonance broadening due to anisotropic ions: the transverse[39,40] and the longitudinal relaxation model.[41–43] Explicit expressions for the latter mechanism for low-spin d^5 ions on octahedral sites have been given previously.[16] Using a very simple temperature dependence of the relaxation time $\tau_{[hkl]}$ which arises from the direct or one-phonon process[44]

$$\tau_{[hkl]} = \tau^0_{[hkl]} \tanh\left(\frac{\hbar\omega_n}{2kT}\right) , \tag{19}$$

the temperature dependence of the linewidth contributions of the Ir^{4+} ions can be calculated. The solid curve in Fig. 10 displays the result for the

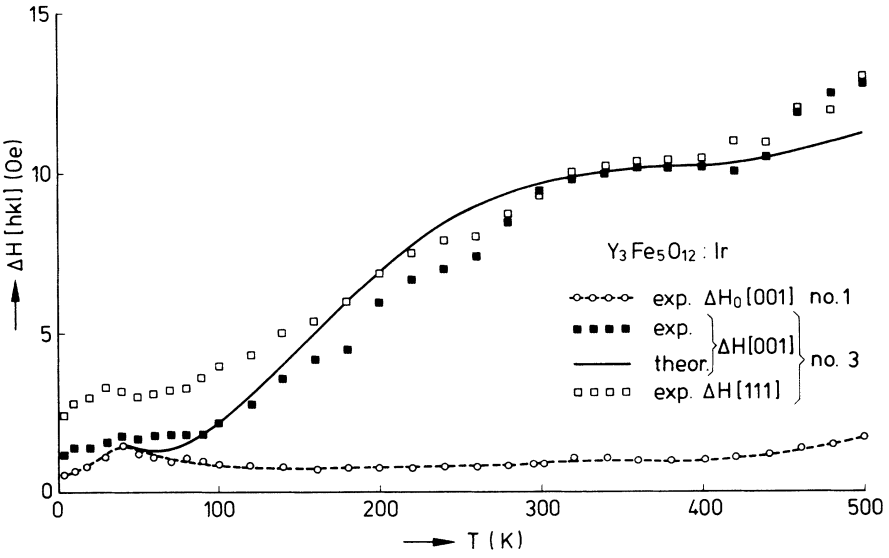

FIG. 10. Temperature dependence of the ferromagnetic-resonance linewidth in [001] and [111] direction. $\Delta H_0[001]$ denotes the linewidth of pure YIG. The theoretical curves are based on the longitudinal relaxation mechanism.

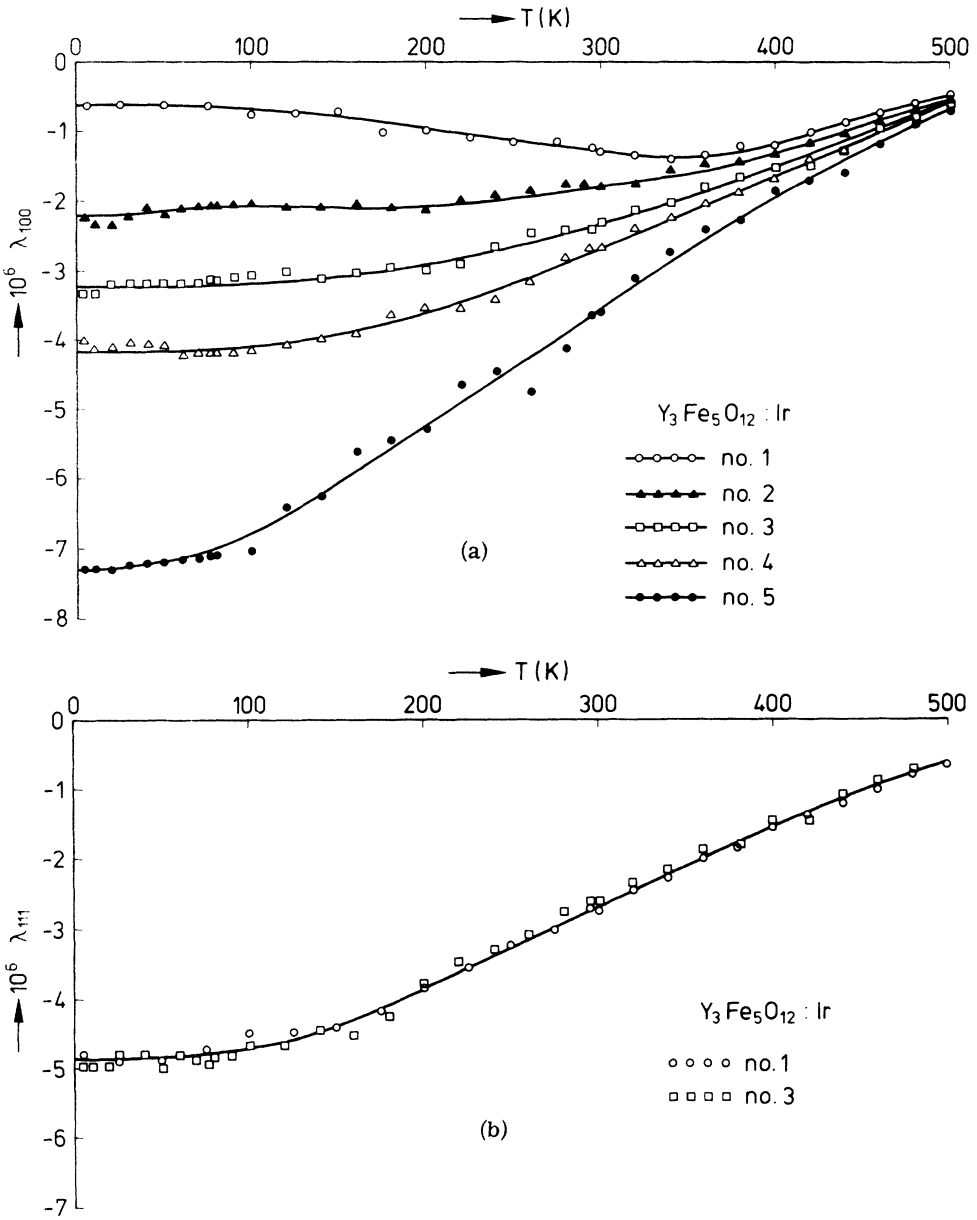

FIG. 11. The influence of low-spin Ir^{4+} ions on octahedral sites on the temperature dependence of the magnetostrictior constants (a) λ_{100} and (b) λ_{111}.

longitudinal process using a relaxation time $\tau^0_{[001]} = 0.9\times10^{-11}$ sec. The curve was fitted at $T = 370$ K using the atomic parameters deduced from the fit of the resonance field. The [111] direction is not suitable for a comparison with theories for reasons of the special level structure in this direction, as discussed in the case of the resonance field. The longitudinal model predicts for the [110] direction a maximum to lower temperatures and the agreement with the experimental data is poorer than in the [001] case.

The transverse mechanism predicts a peak at $\omega_n\tau_{[hkl]} \approx 1$, where $\omega_n = (E_1^+ - E_2^+)/\hbar$. Fitting ΔH_t as $T = 370$ K, a very short relaxation time of $\tau_0 \cong 10^{-14}$ sec is required and then the low-temperature behavior is much less described. Thus the longitudinal process appears to give the better description. However, a real decision between these two models cannot be made, since it was not possible to measure $\Delta H[hkl]$ for different frequencies, and in addition our knowledge about the actual temperature and orientation dependence of the relaxation time is insufficient. Further the valence-exchange mechanism[45] may also cause the linewidth broaden-

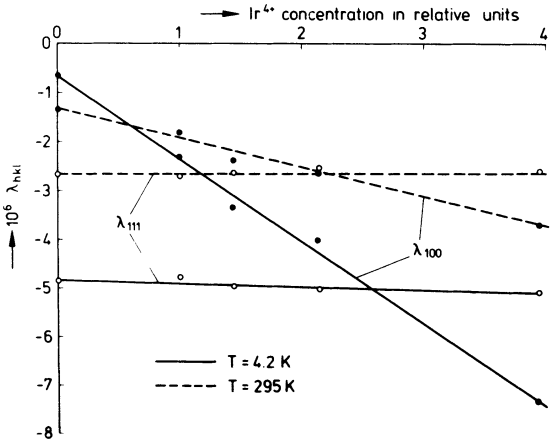

FIG. 12. The concentration dependence of the magnetostriction constants. The spin-wave-linewidth data have been used as a relative measure of the Ir^{4+} concentration (see Table II).

ing, but no experimental evidence could be obtained since, for instance, resistivity measurements were not successful because of the extremely small concentrations of Ir^{4+} ions.

D. Magnetostriction

The magnetostriction measurements were carried out with the resonance method according to Smith and Jones[46,47] and thus were involved in the anisotropy and linewidth measurements with the same conditions discussed before. A compressional uniaxial stress S in the [110] direction has been applied which causes a shift $\delta H_r[hkl]$ in the resonance field $H_r[hkl]$ in the $[hkl]$ direction. The applied stress was between 10^7 and 10^8 dyn cm^{-2}. S has been calculated using an effective area $\frac{2}{3}\pi R^2$ of the spheres. Then the measured values of λ_{100} and λ_{111} of pure YIG are in good agreement with those of other methods.[48,49] From the shifts in the [001] and [110] directions the magnetostriction constants were deduced from the relations[47]

$$\lambda_{100} = -\frac{2}{3}\frac{M_s}{S}\,\delta H_r[001],$$

$$\lambda_{111} = -\frac{4}{9}\frac{M_s}{S}\left(1+\frac{1}{3}\frac{K_2}{M_s H_r[110]}\right)^{-1} \times\left[\left(1-\frac{2K_1-K_2}{4M_s H_r[110]}\right)\delta H_r[110] + \frac{1}{2}\left(1-\frac{2K_1}{M_s H_r[110]}\right)\delta H_r[001]\right]. \tag{20}$$

The linear relationship between $\delta H_r[hkl]$ and S could be verified in all cases. Using the saturation magnetization of pure YIG, λ_{100} and λ_{111} could be calculated from Eqs. (20). The temperature dependence of the magnetostriction constants is plotted in Fig. 11(a) and 11(b). A pronounced effect is observed for λ_{100} while λ_{111} remains approximately unchanged. Fig. 11(b) shows only the measured values of samples No. 1 and 3, since samples No. 2 and 4 show the same temperature behavior. The concentration dependence is shown in Fig. 12 for two temperatures. Here the spin-wave linewidth has been used as a relative measure of the Ir^{4+} concentration because it was not possible to detect it by chemical methods. The actual concentrations estimated from the anisotropy data give rise to quite large contributions per ion (values in the brackets of Table III). A comparison with other ions can be found in Table III.

The observed behavior of the magnetostrictive effect was expected from the single-ion theory, which predicts $|\Delta\lambda_{100}| \gg |\Delta\lambda_{111}|$ for $v/\xi > 0$ assum-

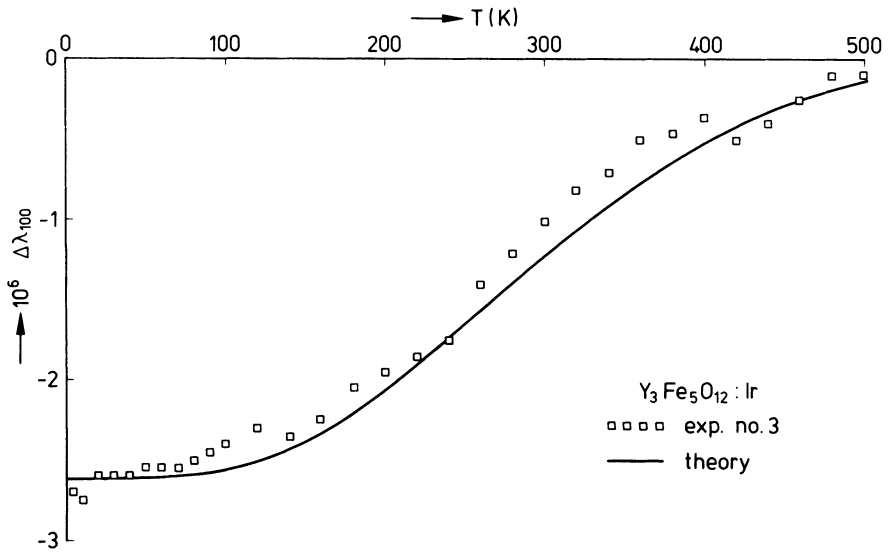

FIG. 13. Temperature dependence of the magnetostriction contribution $\Delta\lambda_{100} = \lambda_{100}(v) - \lambda_{100}(0)$ of the Ir^{4+} ions of sample No. 3. The theoretical curve has been calculated with the values $\xi = 2000$ cm^{-1}, $v/\xi = 0.5$, $gH_e = 1.8\times10^7$ Oe, and $NW_{33} = 5.3\times10^6$ erg cm^{-3}. The elastic constants of pure YIG have been used.

ing that the ratio of the matrix elements W_{12} and W_{33} does not change drastically in comparison with those of Ru^{3+}. These matrix elements are positive for Ru^{3+} in YIG [20] but they are expected to be negative for Ir^{4+} because in this case, obviously, the local trigonal field has an opposite sign. Therefore the magnetostriction contribution is expected to be negative as it has been observed.

For a comparison of the experimental results with the single-ion theory of Sec. II the Ir^{4+} contribution $\Delta\lambda_{100} = \lambda_{100}(y) - \lambda_{100}(0)$ of sample No. 3 has been plotted versus temperature in Fig. 13. λ_{111} will not be considered further since approximately no detectable effect was present. The elastic constants of pure YIG, $C_{11} - C_{12} = 1.61 \times 10^{12}$ erg cm^{-3} at $T = 296$ K, [50] were used to compute $\Delta\lambda_{100}$. The one-electron spin-orbit coupling constant was estimated from the optical-absorption measurements and the anisotropy data to range about $\xi \cong 2000$ cm^{-1}. The quantities v/ξ and gH_e have been deduced from the anisotropy behavior, yielding the values $v/\xi = 0.49$ and $gH_e = 1.8 \times 10^7$ Oe. With these data the temperature dependence is completely determined. Thus only the remaining parameter NW_{33} has to be adjusted at low temperatures, giving the absolute magnitude of the magnetostriction. The solid curve in Fig. 13 has been calculated for $NW_{33} = 5.3 \times 10^6$ erg cm^{-3}, achieving a good fit to the experimental data. The exchange field has been taken as temperature dependent as in the anisotropy case, but its strain dependence has been neglected which might have been important. [51] With the estimated values of the concentration from Table II W_{33} is found to be $W_{33} = -15\,000$ cm^{-1}, which appears to be extremely large and indicates the concentration values to be too small. However, the $5d^5$ ion with the high valency and the strong spin-orbit coupling is expected to give rise to a much larger constant as, for instance, Ru^{3+}, where W_{33} amounts to 2100 cm^{-1}.

IV. CONCLUSION

The presence of low-spin $5d^5$ Ir^{4+} ions in YIG were shown to give a considerable contribution to the optical absorption, the linewidth, the anisotropy, and magnetostriction. Both ΔK_1 and ΔK_2 turn out to be positive and $\Delta K_2 \gg \Delta K_1$. The magnetostriction of iridium-doped YIG is increased and thus both $\Delta\lambda_{100}$ and $\Delta\lambda_{111}$ are negative with $|\Delta\lambda_{100}| \gg |\Delta\lambda_{111}|$. The observed behavior can be well explained in terms of the single-ion model with simplifying assumptions concerning the Hamiltonian, which determines the anisotropic behavior of the lowest energy levels of the Ir^{4+} ions. However, the fit of the theory to the experimental data suggests the local trigonal field to be positive in contrast to $4d^5$ Ru^{3+} in YIG and thus the negative trigonal field of YIG could not be confirmed in this case in contrast to ESR measurements in yttrium gallium garnet. [52] Further, the Ir^{4+} concentration which is necessary to adjust the theory to the experimental data turns out to be much lower than the actual total iridium content. Therefore possibly a distribution of the iridium ions on different crystallographic sites is present.

On the basis of the assumption of a pure octahedral occupation, the exchange field times the g factor gH_e and the ratio v/ξ of the trigonal field parameter to the spin-orbit coupling parameter were extracted from the anisotropy measurements to be 1.8×10^7 Oe and 0.5, respectively. Estimating ξ from the optical absorption and the anisotropy to be of the order 2000 cm^{-1} the trigonal field parameter v is about 1000 cm^{-1}.

The linewidth contributions can be qualitatively interpreted by the longitudinal relaxation mechanism assigning a relaxation time of $\tau_0 \cong 10^{-11}$ sec to the Ir^{4+} ions.

ACKNOWLEDGMENTS

The authors wish to express their thanks to Dr. J. Verweel for helpful discussions and to Mrs. E. Haberkamp for the chemical analysis and optical-absorption measurements.

[1] T. S. Hartwick and J. Smit, J. Appl. Phys. **40**, 3995 (1969).
[2] R. W. Teale, D. W. Temple, and D. I. Weatherley, J. Phys. C 3, 1376 (1970).
[3] R. Gerber and G. Elbinger, J. Phys. C 3, 1363 (1970).
[4] P. Hansen, W. Tolksdorf, and J. Schuldt, J. Appl. Phys. **43**, 4740 (1972).
[5] J. Smit, E. K. Lotgering, and R. P. Van Stapele, J. Phys. Soc. Jap. Suppl. **17**, 268 (1962).
[6] J. C. Slonczewski, Phys. Rev. **110**, 1341 (1958).
[7] J. C. Slonczewski, Phys. Rev. **122**, 1367 (1961).
[8] T. Okada, H. Sekizawa, and S. Iida, J. Phys. Soc. Jap. **18**, 981 (1963).
[9] M. D. Sturge, E. M. Gyorgy, R. C. LeCraw, and J. P. Remeika, Phys. Rev. **180**, 413 (1969).
[10] M. Rosenbloom and R. W. Teale, J. Phys. C 4, 537 (1971).
[11] G. F. Dionne and J. B. Goodenough, Mater. Res. Bull. **7**, 749 (1972).
[12] R. Krishnan, Phys. Status Solidi **1**, K17 (1970).
[13] P. Hansen, Philips Res. Rep. Suppl. 7, 1 (1970).
[14] P. Hansen, Phys. Rev. B **3**, 862 (1971).
[15] R. Krishnan, Phys. Status Solidi A **4**, K177 (1971).
[16] P. Hansen, Phys. Rev. B **5**, 3737 (1972).
[17] P. Hansen, Phys. Status Solidi B **47**, 565 (1971).
[18] P. Hansen and W. Tolksdorf, Int. J. Magn. **3**, 81 (1972).
[19] R. Krishnan, V. Cagan, and M. Rivoire, AIP Conf. Proc. (5), 704 (1971).
[20] P. Hansen, Phys. Rev. B 8, 246 (1973).
[21] R. D. Shannon and C. T. Prewitt, Acta Crystallogr. B **25**, 925 (1969).
[22] L. E. Orgel, *Introduction to Transition-Metal Chemistry Ligand-Field Theory* (Wiley, New York, 1960).
[23] P. Hansen and W. Tolksdorf, Phys. Status Solidi A **6**, K11 (1971).
[24] K. Yosida and M. Tachiki, Prog. Theor. Phys. **17**, 331

(1957).
[25]W. P. Wolf, Phys. Rev. **108,** 1152 (1957).
[26]K. W. H. Stevens, Proc. R. Soc. A **219,** 542 (1953).
[27]P. Hansen, J. Appl. Phys. **43,** 650 (1972).
[28]T. Asada and H. Miwa, J. Phys. Soc. Jap. **33,** 936 (1972).
[29]C. J. Ballhausen, *Introduction to Ligand-Field Theory* (McGraw-Hill, New York, 1962).
[30]The value for Ir^{4+} of Fig. 2 has been obtained averaging the experimental values from Ref. 13 and the present work.
[31]G. V. Chester, Phys. Rev. **93,** 606 (1954).
[32]W. Tolksdorf, J. Cryst. Growth **3,** 463 (1968).
[33]W. Tolksdorf and F. Welz, J. Cryst. Growth **13,** 566 (1972).
[34]B. Andlauer, J. Schneider, and W. Tolksdorf, Phys. Rev. B 8, 1 (1973).
[35]B. Johnson and A. K. Walton, Br. J. Appl. Phys. **16,** 475 (1965).
[36]G. A. Petrakovskii, I. K. Pukhov, V. N. Seleznev, and A. I. Drokin, Instrum. Exp. Tech. **2,** 1522 (1969).
[37]E. E. Anderson, Phys. Rev. **134,** A1581 (1964).
[38]G. F. Dionne, J. Appl. Phys. **41,** 4874 (1970).
[39]P. G. de Gennes, C. Kittel, and A. M. Portis, Phys. Rev. **116,** 323 (1959).
[40]J. H. Van Vleck, J. Appl. Phys. **35,** 882 (1964).
[41]R. W. Teale and K. W. Tweedale, Phys. Lett. **1,** 298 (1962).
[42]J. H. Van Vleck and R. Orbach, Phys. Rev. Lett. **11,** 65 (1963).
[43]F. Hartmann-Boutron, J. Appl. Phys. **35,** 889 (1964).
[44]R. Orbach, Proc. R. Soc. A **264,** 458 (1961).
[45]A. M. Clogston, Bell Syst. Tech. J. **34,** 739 (1955).
[46]A. B. Smith and R. V. Jones, J. Appl. Phys. **34,** 1283 (1963).
[47]A. B. Smith, Rev. Sci. Instrum. **39,** 378 (1968).
[48]E. DeLacheisserie and J. L. Dormann, Phys. Status Solidi **35,** 925 (1969).
[49]E. R. Callen, A. E. Clark, B. DeSavage, W. Coleman, and H. B. Callen, Phys. Rev. **130,** 1735 (1963).
[50]A. E. Clark and R. E. Strakna, J. Appl. Phys. 32, 1172 (1961).
[51]J. A. Hodges and F. Chantereau, J. Phys. (Paris) (to be published).
[52]E. L. Offenbacher and H. Waldman, Bull. Am. Phys. Soc. 13, 435 (1968).